BIOCHEMISTRY
including biophysical chemistry & molecular biology

Article

pubs.acs.org/biochemistry

A Conserved Acidic Residue in Phenylalanine Hydroxylase Contributes to Cofactor Affinity and Catalysis

Judith A. Ronau,[†,‡] Lake N. Paul,[§] Julian E. Fuchs,[∥,⊥] Klaus R. Liedl,[∥] Mahdi M. Abu-Omar,[†] and Chittaranjan Das*[,†]

[†]Department of Chemistry, Purdue University, 560 Oval Drive, West Lafayette, Indiana 47907, United States

[‡]Department of Molecular Biophysics and Biochemistry, Yale University, 266 Whitney Avenue, New Haven, Connecticut 06520, United States

[§]Bindley Biosciences Center, Purdue University, West Lafayette, Indiana 47907, United States

[∥]Institute of General, Inorganic and Theoretical Chemistry and Center for Molecular Biosciences Innsbruck (CMBI), University of Innsbruck, Innrain 80/82, 6020 Innsbruck, Austria

[⊥]Centre for Molecular Informatics, Department of Chemistry, University of Cambridge, Lensfield Road, Cambridge CB2 1EW, United Kingdom

Supporting Information

ABSTRACT: The catalytic domains of aromatic amino acid hydroxylases (AAAHs) contain a non-heme iron coordinated to a 2-His-1-carboxylate facial triad and two water molecules. Asp139 from *Chromobacterium violaceum* PAH (cPAH) resides within the second coordination sphere and contributes key hydrogen bonds with three active site waters that mediate its interaction with an oxidized form of the cofactor, 7,8-dihydro-L-biopterin, in crystal structures. To determine the catalytic role of this residue, various point mutants were prepared and characterized. Our isothermal titration calorimetry (ITC) analysis of iron binding implies that polarity at position 139 is not the sole criterion for metal affinity, as binding studies with D139E suggest that the size of the amino acid side chain also appears to be important. High-resolution crystal structures of the mutants reveal that Asp139 may not be essential for holding the bridging water molecules together, because many of these waters are retained even in the Ala mutant. However, interactions via the bridging waters contribute to cofactor binding at the active site, interactions for which charge of the residue is important, as the D139N mutant shows a 5-fold decrease in its affinity for pterin as revealed by ITC (compared to a 16-fold loss of affinity in the case of the Ala mutant). The Asn and Ala mutants show a much more pronounced defect in their k_{cat} values, with nearly 16- and 100-fold changes relative to that of the wild type, respectively, indicating a substantial role of this residue in stabilization of the transition state by aligning the cofactor in a productive orientation, most likely through direct binding with the cofactor, supported by data from molecular dynamics simulations of the complexes. Our results indicate that the intervening water structure between the cofactor and the acidic residue masks direct interaction between the two, possibly to prevent uncoupled hydroxylation of the cofactor before the arrival of phenylalanine. It thus appears that the second-coordination sphere Asp residue in cPAH, and, by extrapolation, the equivalent residue in other AAAHs, plays a role in fine-tuning pterin affinity in the ground state via deformable interactions with bridging waters and assumes a more significant role in the transition state by aligning the cofactor through direct hydrogen bonding.

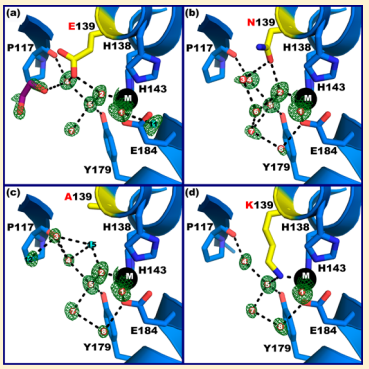

Aromatic amino acid hydroxylases (AAAHs) constitute a family of pterin-dependent monooxygenases, including phenylalanine hydroxylase (PAH), tyrosine hydroxylase (TH), and tryptophan hydroxylase (TPH).[1−3] Mammalian AAAHs share similar structural elements in that they exist as homotetramers in which each monomeric unit is comprised of three domains: an N-terminal regulatory domain, a catalytic domain, and a C-terminal tetramerization domain.[4,5] The active site of AAAHs, housed in the catalytic domain of the enzyme, coordinates with Fe(II) to drive the reaction via a facial catalytic triad (His, His, and Glu), consistent with 2-His-1-carboxylate triads found in similar metalloproteins.[6] These mononuclear non-heme iron(II)-containing enzymes utilize a pterin cofactor (6*R*)-L-*erythro*-5,6,7,8-tetrahydrobiopterin (BH_4) and dioxygen to oxidize target aromatic amino acids.[7] During the hydroxylation reaction, BH_4 is also subjected to a two-electron oxidation, generating 4a-hydroxytetrahydrobiopterin, which is then recycled to BH_4 with the aid of two enzymes. First, 4a-carbinolamine dehydratase dehydrates 4a-hydroxytetrahydrobiopterin to quinonoid dihydropterin (dehydration can also proceed nonenzymatically, owing to a reasonably rapid rate in the absence of enzyme), which, in turn, is reduced to BH_4 by

Received: June 12, 2014
Revised: September 22, 2014
Published: October 8, 2014

   dx.doi.org/10.1021/bi500734h | *Biochemistry* 2014, 53, 6834−6848

Scheme 1. Hydroxylation of Phenylalanine to Tyrosine by Phenylalanine Hydroxylase (PAH) Results in Two-Electron Oxidation of the Cofactor, Tetrahydrobiopterin (BH_4)[a]

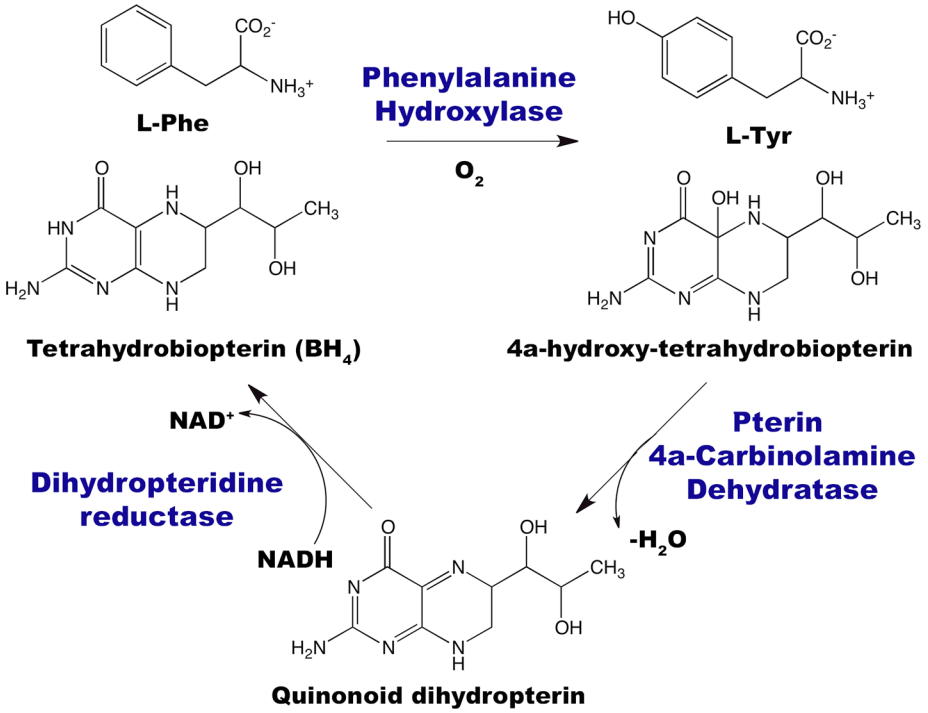

[a]The oxidized form of the cofactor, 4a-hydroxytetrahydrobiopterin, is recycled to BH_4 with the aid of two enzymes, pterin 4a-carbinolamine dehydratase and dihydropteridine reductase.

the NADH-dependent enzyme dihydropteridine reductase (Scheme 1).[8]

In particular, phenylalanine hydroxylase (PAH) is a crucial metabolic enzyme responsible for conversion of dietary phenylalanine to tyrosine, serving two key purposes. Hydroxylation of phenylalanine in eukaryotic organisms represents the only pathway toward generation of tyrosine, an amino acid that serves as a precursor for neurotransmitters[9] and as a building block in protein synthesis.[10,11] Furthermore, organisms with properly functioning PAH avoid detrimental side reactions that lead to formation of undesirable phenylalanine derivatives, such as phenylpyruvate,[12] a scenario that surfaces when phenylalanine accumulates. Phenylketonuria (PKU), a genetic disease leading to irreversible brain damage in children, arises in humans when PAH is defective.[13,14]

Several X-ray crystal structures of AAAH family members in complex with pterin cofactors [PAH from *Chromobacterium violaceum* (cPAH),[15] human PAH,[16,17] human TH,[18] rat TH,[19] and human TPH[20]] illustrate the contacts that are made with the enzyme upon cofactor binding (Figure 1a–e), confirming previous proposals that the pterin binding site is highly conserved among all AAAHs.[1,21] For example, in cPAH, two loop regions (residues 98–103 and 245–250), the main chain atoms of proline 117, and the side chains of tyrosine 179 and aspartic acid 139 are involved in pterin binding.[15] Prior mutational studies of second-coordination sphere residue Y179 in cPAH[22] and the homologous amino acid Y325[23] in hPAH indicate that while it has an effect on pterin binding, its contribution to phenylalanine binding is more pronounced. Furthermore, another study showed Y325 in hPAH plays a role in stoichiometric binding of iron and cooperative regulation by phenylalanine.[24]

The acidic, negatively charged residue at position 139 in cPAH is highly conserved among other PAHs, as well as within the entire AAAH family (Figure 1f). Interestingly, unlike the majority of AAAHs in which glutamic acid occupies this position, in cPAH, the residue in this position is instead aspartic acid. In the crystal structure of cPAH and an oxidized form of the cofactor, 7,8-dihydrobiopteirn (BH_2), three water molecules bridge the interaction between D139 and the cofactor (Figure 1a);[15] one of the waters also occupies a coordination site on iron. On the basis of the crystal structure of hPAH bound to the fully reduced form of its cofactor, BH_4 [Protein Data Bank (PDB) entry 1J8U],[25] it is evident that E286 associates with pterin through two water-mediated contacts, in a manner similar to that of cPAH D139 (Figure 1b). Inclusion of thienylalanine (THA), a substrate analogue for phenylalanine, causes displacement of the bridging water molecules in the crystal structure (PDB entry 1KW0),[26] resulting in direct hydrogen bonding between E286 and pterin (Figure 1c). Furthermore, THA binding in the active site results in pterin being repositioned 2.6 Å closer to iron,[26] likely representing its orientation during the enzyme-catalyzed hydroxylation reaction. In the crystal structure of oxidized pterin (BH_2) in complex with rat tyrosine hydroxylase, the cofactor adopts a flipped conformation such that the dihydroxpropyl chain of the cofactor is oriented toward Glu332 (the second-coordination sphere residue analogous to Asp139 in cPAH) and the water molecules seen bridging pterin and the acidic amino acid are thus lost (Figure 1d).[19] Tryptophan hydroxylase (TrpOH) also has been crystallized with BH_2. Like hPAH, TrpOH also binds to BH_2 through two water-mediated contacts (Figure 1e).[20]

With a goal of further understanding the catalytic contribution made by the conserved acidic amino acid residing in the second-coordination sphere of an aromatic amino acid

dx.doi.org/10.1021/bi500734h | *Biochemistry* 2014, 53, 6834–6848

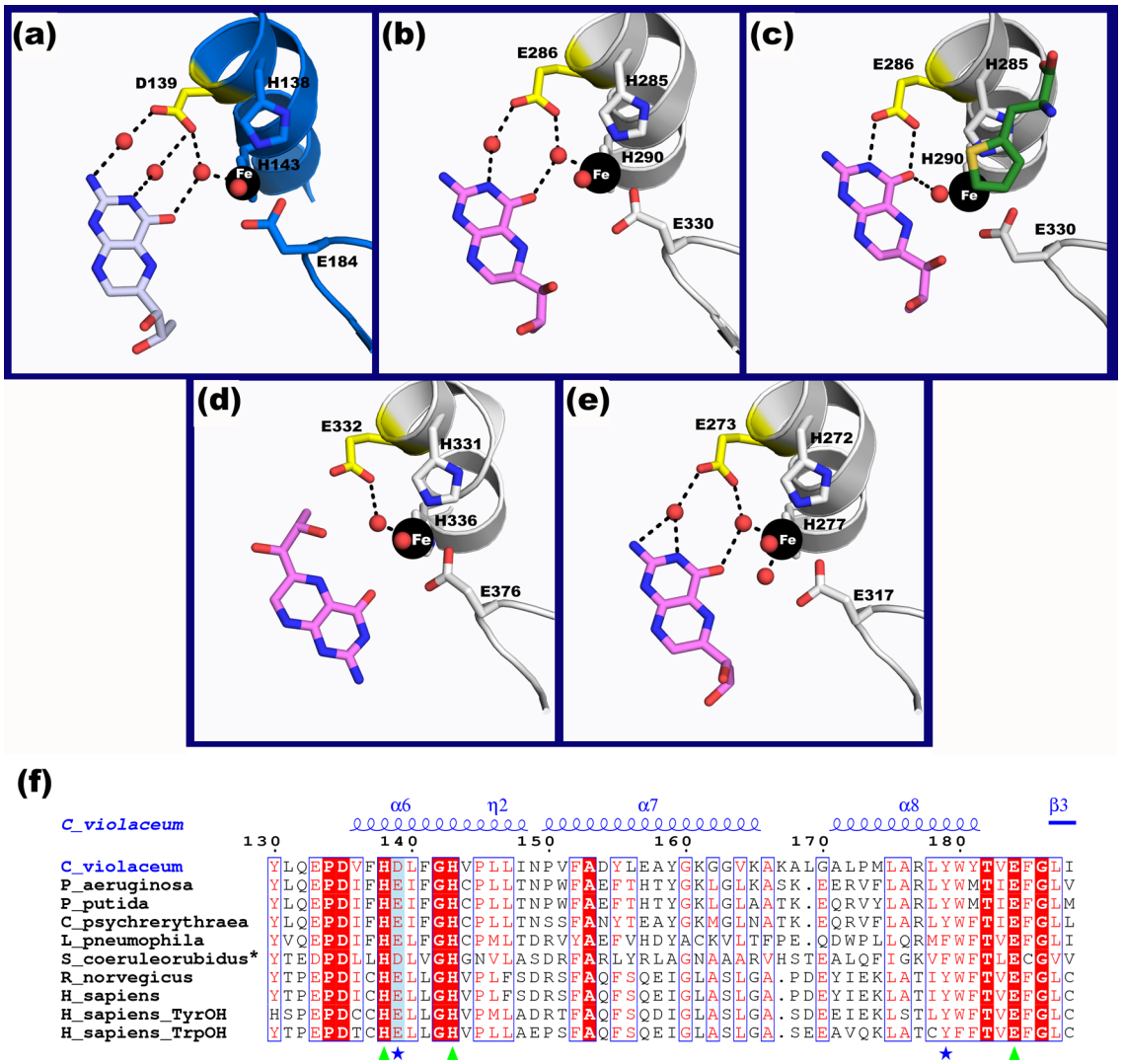

Figure 1. Acidic residue at position 139 in cPAH that is conserved in mammalian PAH and in other AAAHs. (a) The crystal structure of cPAH bound to iron and pterin (PDB entry 1LTZ) shows D139 (yellow) hydrogen bonds with pterin (white) through three bridging water molecules (red spheres). (b) A similar water-mediated interaction is observed in the crystal structure of hPAH in its binary complex (PDB entry 1J8U), which is pushed out in favor of direct interaction between E286 and pterin (c) when a substrate analogue, thienylalanine (THA), is bound in the active site (PDB entry 1KW0). (d) Cocrystal structure of rat tyrosine hydroxylase bound to pterin (PDB entry 2TOH). (e) Cocrystal structure of tryptophan hydroxylase bound to pterin (PDB entry 1MLW). (f) Sequence alignment of cPAH, mammalian PAHs, and other AAAHs, showing conservation of an acidic residue at position 139 in cPAH, which is Glu in most other AAAHs but Asp in cPAH (blue star, light blue shaded box). Asterisks indicate *Streptomyces coeruleorubidus* PAH generates meta-hydroxylated tyrosine.

hydroxylase, we investigated mutants of cPAH aspartic acid 139. The rationale for using cPAH in this study is based on the following observations. First, despite the fact that, unlike eukaryotic PAHs, cPAH is a monomeric enzyme consisting of only a single (catalytic) domain, its structure shares a similar fold with not only hPAH[27,28] but also TH and TPH, therefore enabling its use as a model for AAAHs in general. Moreover, allosteric activation by substrate has not been demonstrated in cPAH.[29,30] However, it should be noted that with the discovery of a second phenylalanine binding site in cPAH,[31] the idea that it too may be regulated in some way cannot be ruled out. We hypothesized that the contribution of this negatively charged residue to catalysis is multifaceted; the charge could be important in localization and stabilization of iron, and the charge could be playing a key role in positioning and stabilizing the cofactor in the transition state. The corresponding residue in hPAH, E286, has been studied kinetically using two constructs of hPAH: hPAHN[122] and hPAHN[102]/C[24]; both studies concluded that E286 was important in positioning the cofactor.[17,32] Because E286 forms a hydrogen bond with one water that also coordinates iron, Dickson et al. ruled out the possibility that impaired metal binding contributed to decreased enzymatic activity in their study. Moreover, it has been proposed that the negative charge of Asp139 could be essential in the stabilization of the positive charge in the pyrimidine ring of the peroxy−pterin intermediate.[33] Despite finding the conserved second-coordination sphere Glu/Asp important in catalysis, no mechanistic insight was gained from these studies. More importantly, previous studies lacked structural data in support of the change in water structure that may be associated with mutation. In this work, we investigated the contribution of Asp139 by generating point mutants (D139N, D139E, D139A, and D139K) to probe several aspects of cofactor and substrate binding and catalysis.

dx.doi.org/10.1021/bi500734h | *Biochemistry* 2014, 53, 6834−6848

Table 1. Crystallographic Data Collection and Refinement Statistics for D139 Mutants of cPAH

	D139N	D139A	D139E	D139K
		Data Collection[a]		
space group	*P*1	*P*1	*P*1	*P*1
cell dimensions				
a, *b*, *c* (Å)	36.8, 38.5, 47.8	37.0, 38.7, 47.9	37.0, 38.7, 47.8	36.8, 35.6, 47.7
α, *β*, *γ* (deg)	76.5, 73.1, 85.6	76.7, 72.8, 85.5	76.7, 72.9, 85.6	76.6, 72.8, 85.5
resolution (Å)	50.0−1.35 (1.37−1.35)	50.0−1.40 (1.42−1.40)	50.0−1.40 (1.42−1.40)	50.0−1.35 (1.37−1.35)
R_{merge}[b] (%)	5.6 (45.5)	6.7 (49.9)	9.1 (56.9)	6.8 (48.7)
$I/\sigma I$	17.9 (3.4)	18.3 (3.0)	15.4 (2.2)	15.9 (3.3)
completeness (%)	95.3 (92.5)	95.8 (92.9)	95.8 (93.1)	95.4 (92.8)
redundancy	4.0 (3.9)	3.9 (3.6)	3.9 (3.8)	4.0 (3.8)
		Refinement		
resolution (Å)	1.35	1.40	1.40	1.35
no. of reflections	48311	43948	43956	48263
R_{work}[c]/R_{free}[d]	16.2/20.0	16.7/20.5	16.0/19.7	16.2/19.8
no. of atoms				
protein	2148	2145	2230	2155
ion	1	1	1	1
water	177	164	190	136
root-mean-square deviation				
bond lengths (Å)	0.007	0.007	0.007	0.010
bond angles (deg)	1.260	1.281	1.257	1.403
average *B* factor (Å^2)				
protein	16.8	15.5	16.1	17.1
ion	7.2	7.3	8.1	8.0
water	28.7	26.1	28.3	28.1
ligand	–	–	–	–

[a]Values in parentheses are for the highest-resolution shell. [b]$R_{merge} = \sum\sum|I_{hkl} - I_{hkl(j)}|/\sum\sum I_{hkl}$, where $I_{hkl(j)}$ is the observed intensity and I_{hkl} is the final average intensity. [c]$R_{work} = \sum||F_{obs}| - |F_{calc}||/\sum|F_{obs}|$. R_{work} values were calculated using all reflections excluding the 5% test data. [d]$R_{free} = \sum||F_{obs}| - |F_{calc}||/\sum|F_{obs}|$. R_{free} values were calculated using a randomly selected test set of 5% of the data.

Unlike previous studies, we used isothermal titration calorimetry to study binding of ferrous iron, reduced pterin cofactor, and phenylalanine in the enzyme's active site. We also used high-resolution X-ray crystallography and molecular dynamics simulations of mutants to correlate structural changes in the active site (especially ordered solvent) with activity.

METHODS

Cloning of Mutant Enzymes. All point mutations of cPAH (D139A, D139N, D139E, D139K, and D139H) were prepared using *AccuPower* PCR PreMix (Bioneer). The primers used for mutagenesis were D139A (forward), 5′-GACGTGT-TCCACG*C*CCTGTTCGGCCAC-3′, D139N (forward), 5′-GACGTGTTCCAC*A*ACCTGTTCGGCCAC-3′, D139K (forward), 5′-GACGTGTTCCAC*AAA*CTGTTCGGCCAC-3′, D139E (forward), 5′-GACGTGTTCCACGA*A*CTGTTCGG-CCAC-3′, and D139H (forward), 5′-GACGTGTTCCAC*C*A-CCTGTTCGGCCAC-3′ (mismatched nucleotides are represented in boldface and italics). Mutations were verified by DNA sequencing.

Protein Expression and Purification. Wild-type and mutant cPAH forms were purified from a pET3a vector in the absence of an affinity tag as described previously.[30,31] A large-scale culture was grown to late log phase and induced with 1 mM isopropyl *β*-D-1-thiogalactopyranoside. Following induction at 18 °C for 16 h, cells were harvested and lysed via a French press. The protein was then purified by a combination of anion-exchange chromatography and size-exclusion chromatography. Enzymes were concentrated, buffer-exchanged into 50 mM Na-HEPES (pH 7.4), and stored at −80 °C. The protein concentration was determined via UV−vis spectroscopy.

Kinetics. The hydroxylation of phenylalanine was assayed using a Shimadzu UV-2501 double-beam spectrophotometer equipped with a thermostat-controlled cuvette holder by monitoring the production of tyrosine at 275 nm (ε_{275} = 1405 L mol^{-1} cm^{-1}). All assays were conducted at 20 ± 1 °C. The enzyme concentration used in assays varied from 1 *μ*M wild-type cPAH to 30 *μ*M D139A. Assays also contained a 5-fold excess of ferrous ammonium sulfate ($FeSO_4$) with respect to enzyme concentration, 5 mM dithiothreitol, 1000 units/mL bovine catalase, varied concentrations of tetrahydropterin cofactor, 6,7-dimethyl-5,6,7,8-tetrahydropterine ($DMPH_4$) at saturated Phe (1 mM), and varied concentrations of Phe at saturated $DMPH_4$ (350 *μ*M), in 0.1 M O_2-saturated Na-HEPES (pH 7.4). All assays were conducted in triplicate, and kinetic data were fit to the Michaelis−Menten equation $v_i = (V_{max}[S])/(K_M + [S])$ using Kaleidagraph. Data are given as means ± the standard deviation from three independent experiments.

Crystallization and Data Collection. Crystallization of mutants under study was carried out as described previously.[31] Crystals were grown from microseeds of wild-type protein in 5 *μ*L drops (2 *μ*L of protein, 2 *μ*L of reservoir solution, 0.4 *μ*L of hexamine cobalt(III) chloride additive, 0.4 *μ*L of guanidine hydrochloride additive, and 0.2 *μ*L of seeds) using the hanging drop vapor diffusion method. Crystals were cryoprotected by being soaked in 25% ethylene glycol and then flash-frozen in liquid nitrogen. Data from mutant crystals D139A (1.40 Å), D139N (1.35 Å), and D139K (1.35 Å) were collected on GM/CA beamlines at the Advanced Photon Source at Argonne

dx.doi.org/10.1021/bi500734h | *Biochemistry* 2014, 53, 6834−6848

Table 2. Steady-State Kinetic Parameters for Aspartic Acid 139 Mutants of Phenylalanine Hydroxylase

	DMPH		L-Phe		
cPAH	K_M (μM)	k_{cat}/K_M ($\times 10^{-3}$ μM^{-1} s^{-1})	K_M (μM)	k_{cat}/K_M ($\times 10^{-3}$ μM^{-1} s^{-1})	k_{cat} (s^{-1})
wild type	152 ± 2	130 ± 3	244 ± 41	48 ± 10	18.6 ± 0.1
D139N	262 ± 41	5.1 ± 0.5	316 ± 93	2.8 ± 0.2	1.2 ± 0.1
D139A	254 ± 47	0.8 ± 0.09	137 ± 3	0.59 ± 0.06	0.19 ± 0.01
D139E	236 ± 38	9.4 ± 1	225 ± 35	7.1 ± 0.9	1.9 ± 0.1
D139K	*a*	*a*	*a*	*a*	*a*

[a]Kinetic parameters for D139K could not be determined.

National Laboratory (Argonne, IL). Diffraction data were collected on a Mar300 CCD detector (Mar USA) at 100 K and processed utilizing HKL3000.[34] The crystals contain one molecule per asymmetric unit and belong to the primitive, triclinic *P*1 space group.

Structure Determination. The program molrep[35] from the ccp4 suite[36] was used to determine the structure using a previously published structure of apo-cPAH (PDB entry 1LTU).[15] For molrep, all water molecules and other ions such as iron and chloride were removed from the aforementioned model to limit model bias. Several cycles of refinement and model building proceeded using Refmac5[37] and Coot,[38] respectively. Anisotropic *B* factors were used during the refinement of all D139 mutant structures. Weights were also optimized during the refinement process. The crystallographic data and refinement statistics are listed in Table 1. All figures were rendered with PYMOL (version 1.5.0.4).[39]

Molecular Dynamics Simulations. We performed unrestrained molecular dynamics simulations of 10 systems to investigate cofactor binding and resulting hydrogen bonding networks *in silico*. Therefore, we constructed (6*R*)-5,6,7,8-tetrahydrobiopterin (BH_4)-bound systems for native cPAH and four mutants (D139A, D139E, D139K, and D139N) by superposition of respective apo structures with the BH_4-bound enzyme (PDB entry 1LTZ).[15] We modeled an unresolved loop region remote from the active site based on the complete D139E structure (residues 126−134). We discarded bound ethylene glycol residues as well as water molecules showing van der Waals clashes with the cofactor in the modeled complex (r = 1.5 Å). On the basis of these five systems, we built 10 topologies in complex with Fe(II) and Co(II) ions. After protein preparation using protonate3d,[40] systems were solvated in a truncated octahedral box of TIP4P water molecules with a minimal wall distance of 8.0 Å.[41] The D139K mutants were prepared with a neutral lysine residue to allow coordination to the metal ions.

Simulations were performed using the GPU implementation of pmemd[42] in AMBER14.[43] Protein atoms were described using the AMBER force field 99SB-ILDN,[44] and the cofactor BH_4 was parametrized in the Generalized Amber Force Field (GAFF)[45] in analogy to earlier studies of BH_2-bound PAH.[46,47] Atomic point charges for BH_4 were derived by RESP fitting at the Hartree−Fock 6/31G* level in Gaussian03.[48] van der Waals parameters for Fe(II) were taken from an earlier study[47] and fit for Co(II) by a distance scan against a helium atom (r = 1.25 Å; ε = 0.014 kcal mol^{-1} cm^{-1}). Simulations were performed in the *NpT* ensemble at 300 K and 1.0 bar employing a 8.0 Å nonbonded cutoff. The SHAKE algorithm[49] allowed use of a time step of 2 fs. After an extensive equilibration protocol had been employed,[50] unrestrained sampling was conducted for 100 ns, thereby saving 50000 equally spaced snapshots for subsequent analysis.

Analysis of trajectories was performed using ptraj and cpptraj.[51] After ensuring the stability of the simulations, we extracted direct and solvent-mediated hydrogen bonds between residue 139 and BH_4 using cpptraj's default criteria (d < 3.0 Å; α < 135°). Solvation was characterized by analysis of water positions in a cube with an edge length of 2.0 Å centered on initial water positions of the native systems. Interaction energies between residue 139 and BH_4 were calculated from nonbonded interactions of all atom pairs, thus summing electrostatic and van der Waals contributions. Error bars were calculated from splitting the trajectory in 10 parts of 10 ns.

Isothermal Titration Calorimetry. All isothermal titration calorimetry (ITC) experiments were conducted anaerobically under an argon atmosphere at 25 °C using a GE/MicroCal ITC_{200} calorimeter as described previously.[31] In experiments aimed to measure the affinity of cPAH and its mutants for its native metal, Fe(II), 500 μM ferrous ammonium sulfate was prepared in dialysis buffer containing 2.5 mM tris(carboxyethyl)phosphine (TCEP) and titrated into a 50 μM solution of protein also including 2.5 mM TCEP. TCEP was used to keep iron reduced. $FeSO_4$ solutions used in tetrahydropterin and phenylalanine binding experiments were prepared in 10 mM HCl to keep iron in its reduced state. Prior to initiation of the binding experiment, protein samples containing Fe(II) were spotted on pH paper to ensure that the overall sample pH had not been altered as a result of spiking the sample with iron prepared in HCl. To gauge the effect of mutation on binding of tetrahydropterin cofactor BH_4, 1−5 mM solutions of (6*R*)-5,6,7,8-tetrahydrobiopterin dihydrochloride (BH_4) were titrated into a 50 μM solution of protein containing 50 μM $FeSO_4$. BH_4 was used in ITC in favor of the same form of pterin used in kinetics because the binding isotherms for $DMPH_4$ were very poor (refer to Figure 1 of the Supporting Information for a comparison of pterins used in this study). For experiments in which phenylalanine was titrated into the reconstituted enzyme, 1 mM Phe was titrated into 50 μM protein, 50 μM $FeSO_4$, and 200 μM BH_4.

A total of 18 injections, 2 μL/injection, with 180 s between injections, were performed for cPAH and the mutants (D139A, D139K, D139N, and D139E). The data were baseline-corrected with NITPIC[52] and analyzed using the one-site model in SEDPHAT.[53,54] Figures were prepared using GUSSI.

RESULTS

Steady-State Kinetic Analyses of Asp139 Point Mutations. To understand the contribution of the second-coordination sphere residue aspartic acid 139, steady-state kinetic analysis was carried out for the point mutants D139E, D139N, and D139A. The Glu mutation was made because most AAAHs contain a Glu, not Asp, in this position. To explore the importance of the negative charge and/or polarity

from this residue, we mutated Asp to the uncharged, yet polar, Asn and to the positively charged residue, Lys. The Ala mutant was generated to probe the effect of a complete loss of hydrogen bonding and charge in the side chain. We also prepared a His mutant; however, this mutant proved to be insoluble and could not be purified. The kinetic parameters determined for the mutants are significantly different from those of the wild-type enzyme (Table 2). The K_M values for $DMPH_4$ [an analogue of BH_4 widely used in kinetic experiments (Figure 1 of the Supporting Information)] and L-Phe are slightly higher with respect to the wild-type enzyme in D139E, D139N, and D139A; however, the difference is not very significant and does not necessitate distinction from the wild-type enzyme. In contrast, k_{cat} values for the D139 point mutants are markedly lower than those obtained for the wild-type enzyme; the k_{cat} for D139E is 10-fold lower than that of wild-type cPAH, while the k_{cat} values for D139N and D139A are 16- and 100-fold lower, respectively.

The second-order rate constants, k_{cat}/K_M, indicate that all three mutants are catalytically less efficient in conversion of phenylalanine to tyrosine than the wild-type protein. The k_{cat}/K_M data for the substrate $DMPH_4$ reveal decreases of 14-, 25-, and 158-fold in D139E, D139N, and D139A, respectively. Furthermore, the values of k_{cat}/K_M determined for phenylalanine reveal decreases of 7-, 17-, and 81-fold in D139E, D139N, and D139A mutants, respectively.

The ability of cPAH to catalyze the hydroxylation reaction was dramatically impaired in the D139K mutant. We attempted to obtain steady-state kinetic parameters for this mutant; however, nonenzymatic amounts of protein were required to achieve minimal product formation of tyrosine. Therefore, this mutant is deemed inactive.

Iron Binding in Asp139 Mutants. The substantial changes we observed in k_{cat} as a result of mutation of aspartic acid 139 in cPAH raised the possibility that destabilization of iron binding in the active site could be contributing to the reduction in enzymatic activity. We used isothermal titration calorimetry (ITC) as a direct measurement of iron binding in the active site. To prevent the oxidation of iron, these experiments were conducted in an anaerobic glovebox under an argon atmosphere with 2.5 mM TCEP. Experiments performed in the absence of TCEP resulted in poor binding, probably because of some oxidation of iron (data not shown). Dissociation constants and thermodynamic parameters obtained from iron titration experiments with wild-type cPAH and aspartic acid 139 mutants are summarized in Table 3.

Titration of a 10-fold excess of $FeSO_4$ into wild-type apo-cPAH at 25 °C produced a binding isotherm that could be satisfactorily fit to a one-site model yielding a dissociation constant (K_d) value of 151 ± 28 nM and an N_{ITC} (measure of stoichiometry between protein and ligand) value of 0.8 (Figure 2 and Table 3). Comparatively, titration of iron into the D139N mutant yielded a K_d value of 139 ± 62 nM, indicating that the metal binding ability of the enzyme was not lost as a result of mutation. However, mutation of aspartic acid 139 to glutamate and alanine shows a moderate impairment of iron binding (Figure 2 and Table 3), corresponding to an approximate 4-fold increase in K_d for D139E and a 6-fold increase in K_d for D139A. Despite this reduction in metal binding affinity, we hypothesize that because excess iron was added to the enzyme during our steady-state kinetic analysis, the majority of active sites were metalated and therefore did not contribute to the observed reduced activity of the mutants. Furthermore, wild-type cPAH and all three mutants shared similar positive entropy (ΔS) values (16−24 cal mol^{-1}). This observed increase in entropy is consistent with that demonstrated in a prior metal binding study with cPAH[28] from which it was concluded that discharge of water from the active site leading to iron coordination is the cause of the increased entropy upon metalation. This suggests that the water networks in the immediate vicinity of the metal are similar in the D139N, D139A, and D139E mutants to that of the wild-type enzyme.

We attempted to obtain a dissociation constant for iron binding in the active site of the D139K mutant by titrating a solution containing a 10-fold excess of $FeSO_4$, yet no binding was observed (Figure 2 of the Supporting Information). Titration of a solution containing a 20-fold excess of $FeSO_4$ generated a very weak, endothermic binding isotherm and a K_d of 76.5 ± 0.7 μM correlating to an ∼500-fold reduction in binding affinity for iron (Figure 2 and Table 2). From this experiment, it is clear that the effect of the lysine mutation leads to destabilization of iron. This result also explains why we are unable to obtain kinetic information for this mutant: its ability to bind iron in the active site is significantly impaired. Assuming that the other substrates (phenylalanine and pterin) can still bind the active site in a productive orientation, the hydroxylation reaction would not be catalyzed by an enzyme deficient in iron.

Cofactor and Substrate Binding. Because the crystal structure of cPAH in the ternary complex (bound to both iron and its cofactor, pterin) implicates aspartic acid 139 in pterin binding via three water-mediated interactions (PDB entry 1LTZ),[15] we again utilized ITC to assess each mutant's ability to bind (6*R*)-5,6,7,8-tetrahydrobiopterin dihydrochloride (BH_4) to the Fe(II)-bound enzyme (see Methods). As in the iron binding experiments, to keep BH_4 in its reduced state binding experiments were conducted in an anaerobic glovebox under an argon atmosphere. The dissociation constants and thermodynamic parameters are listed in Table 4.

In a previous study, we determined the K_d for binding of BH_4 to iron-reconstituted wild-type cPAH to be 24 ± 2 μM.[31] Titration of D139N and D139A mutant cPAH enzymes, containing iron-reconstituted active sites (see Methods), with a 100-fold excess of BH_4 yielded K_d values corresponding to approximate 5- and 16-fold decreased binding affinities, respectively (Figure 3 and Table 4). The data were fit agreeably to a one-site binding model, yielding N_{ITC} values of 1 for each mutant, indicating that both mutants bind BH_4 in a 1:1 stoichiometry. Unexpectedly, even though the D139E mutant suffered an impairment in its ability to catalyze tyrosine formation, our ITC experiments revealed that it binds pterin approximately 6-fold tighter than the wild-type enzyme (Table 4 and Figure 3).

Table 3. Dissociation Constants and Thermodynamic Parameters for Binding of the Native Metal, Fe(II) in the Active Site of cPAH, and the Aspartic Acid 139 Mutants

sample	K_d (μM)	ΔH (kcal mol^{-1})	ΔS (cal mol^{-1})	N
wild type	0.151 ± 0.03	−4.0 ± 0.1	18	0.8
D139N	0.139 ± 0.06	−4.5 ± 0.3	16	0.7
D139A	0.944 ± 0.17	−2.5 ± 0.1	19	0.9
D139E	0.479 ± 0.17	−1.5 ± 0.1	24	0.8
D139K	76.5 ± 0.7	1.4 ± 0.6	23	1

dx.doi.org/10.1021/bi500734h | *Biochemistry* 2014, 53, 6834−6848

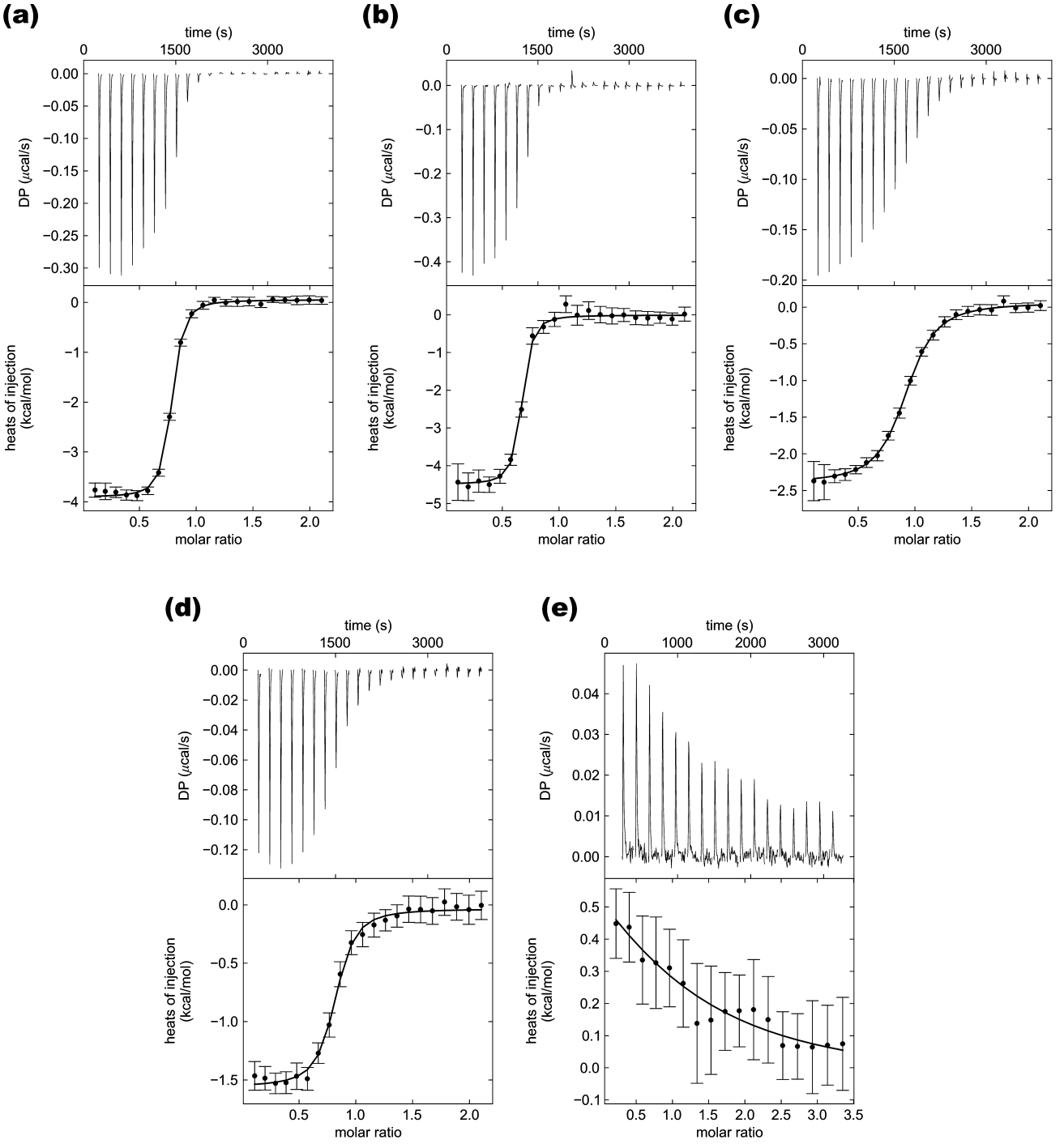

Figure 2. Representative ITC binding thermograms for binding of Fe(II) to (a) wild-type cPAH, (b) D139N, (c) D139A, (d) D139E, and (e) D139K. The experiments were performed in an oxygen-free glovebox under an argon atmosphere to prevent oxidation of iron.

We also observed some interesting entropic changes with the Glu mutant in comparison to the wild-type enzyme upon BH_4 binding. The mutant experienced a positive change in entropy larger than that of the wild-type enzyme, with a ΔS of 7.4 cal mol^{-1} K^{-1}, as compared to a negligible change in ΔS for the wild-type enzyme (−0.4 cal mol^{-1} K^{-1}) upon BH_4 binding (Table 4). Although such a change could mean that the mutant is more solvated in the pterin binding site than the wild type, it could also be taken as an indication that more ordered water molecules have been expelled from the local environment of the Glu side chain to accommodate BH_4 binding.[55,56]

We attempted to obtain a dissociation constant for binding of BH_4 in the D139K mutant but did not observe a binding isotherm for this reaction (Figure 2 of the Supporting Information). Interestingly, mutation of aspartic acid 139 to lysine results in a loss of the enzyme's ability to bind not only iron (as discussed above) but also BH_4, which may explain why this mutant no longer behaves as a catalyst for hydroxylation of phenylalanine (Table 2).

dx.doi.org/10.1021/bi500734h | *Biochemistry* 2014, 53, 6834−6848

Table 4. Thermodynamic Parameters Obtained via ITC for BH_4 and L-Phe Active Site Binding to cPAH and Aspartic Acid 139 Mutants

	BH_4				L-Phe			
sample	K_d (μM)	ΔH (kcal mol^{-1})	ΔS (cal mol^{-1})	N	K_d (μM)	ΔH (kcal mol^{-1})	ΔS (cal mol^{-1})	N
wild type[a]	24 ± 2	−6.4 ± 0.4	−0.4	0.7	37 ± 0.3	−7.9 ± 0.8	−6	0.8
D139N	124 ± 41	−5.8 ± 0.4	−1.5	0.8	37 ± 3.7	−8.5 ± 0.7	−8	0.9
D139A	378 ± 59	−2.2 ± 0.5	8	1	39 ± 12	−10.5 ± 1.9	−15	1
D139E	4.1 ± 0.6	−5.2 ± 0.3	7.4	0.7	55 ± 18	−13.2 ± 6.0	−25	0.6
D139K	N.B.	N.B.	N.B.	N.B.	31 ± 5	−9.4 ± 1.3	−11	0.8

[a]The values for binding of wild-type cPAH to both BH_4 and L-Phe were obtained in a previous study.[31]

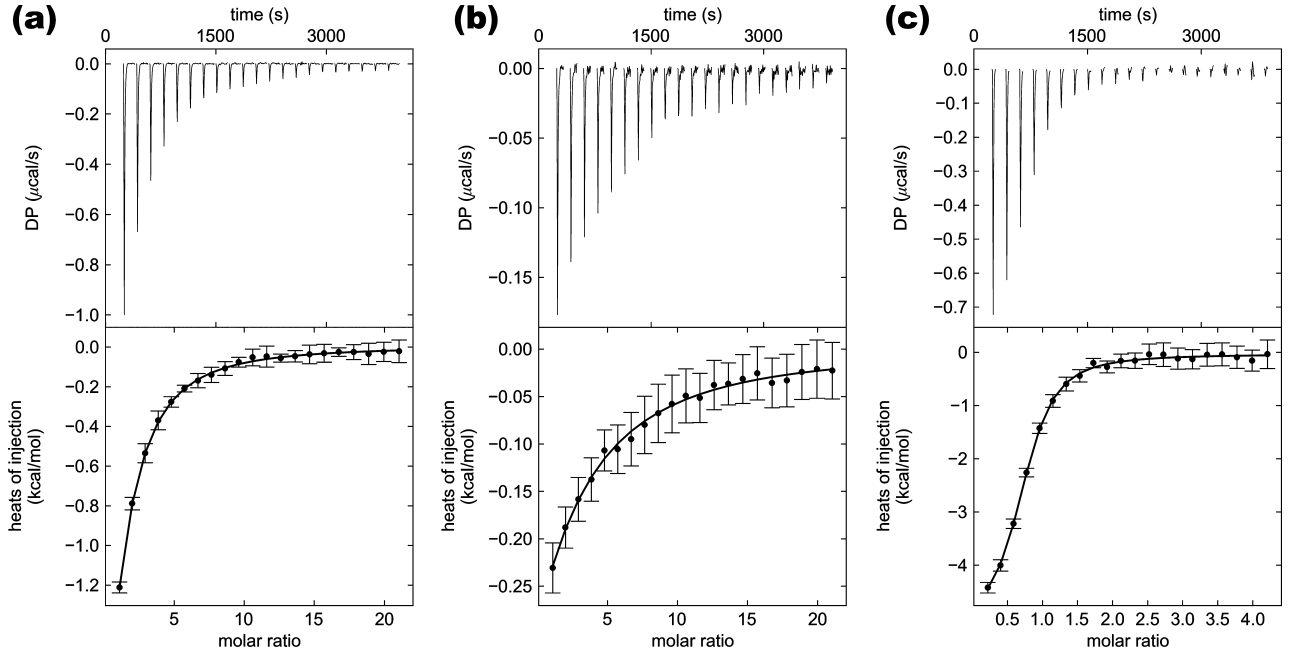

Figure 3. Representative binding isotherms for binding of BH_4 to (a) D139N, (b) D139A, and (c) D139E. To keep BH_4 and iron in their reduced form, experiments were conducted under an argon atmosphere. Titration of BH_4 with D139K failed to generate a binding isotherm.

We conducted phenylalanine binding experiments to rule out the possibility that changing the side chain of a residue implicated in cofactor binding can also affect the enzyme's ability to bind substrate. These experiments were conducted anaerobically, in which a 20-fold excess of phenylalanine was titrated into a solution containing iron-reconstituted cPAH and excess BH_4. As expected, we did not notice a change in phenylalanine binding in D139N, D139A, D139E, or D139K (Figure 4 and Table 4). It is interesting to note that despite having little affinity for iron or BH_4, the D139K mutant binds phenylalanine with the same affinity as wild-type cPAH. These data rule out the idea that the decreased enzyme efficiency seen with D139A and D139N mutants could be the result of impaired phenylalanine binding and also indicate that the presence of a cofactor and/or iron in the active site does not contribute to phenylalanine binding.

Molecular dynamics simulations allowed estimation of the interaction energies between residue 139 and the cofactor BH_4 (see Figure 3 of the Supporting Information). We found strong favorable interactions in the native system and the D139E mutant with interaction energies ranging from −3.3 and −5.8 kcal/mol correlating with experimental binding affinities. Interactions in the D139K mutant are slightly favorable, whereas molecular interactions in mutants D139A and D139N are consistently repulsive with energies in the range of 0.3−1.3 kcal/mol. Presented values reflect only direct interactions between the residues; thus, effects on water networks are not captured as are effects of deprotonation, which is expected for the neutral lysine side chain in mutant D139K.

Solvation Changes in the Active Site. To understand the effect of each mutation on the local active site environment, especially with respect to changes in the water network of the pterin binding pocket, we obtained high-resolution X-ray crystal structures of each mutant. Crystallographic data are summarized in Table 1. Crystals of D139N and D139K diffracted to 1.35 Å resolution, while crystals of D139A and D139E diffracted to 1.40 Å resolution. Molecular replacement was employed to determine the structures, utilizing a previously determined apo-cPAH structure (PDB entry 1LTU)[15] as a search model, with waters deleted. As described previously,[31] cobalt was modeled into electron density representing bound metal coordinated in the active site by residues His138, His143, and Glu184. Crystallographic data for D139N were refined to R_{crys} and R_{free} values of 16.2 and 20.0%, respectively (Table 1). The free R factors for D139A, D139E, and D139K were within 3.6−4.0% of crystallographic R factors.

As discussed earlier, the pterin cofactor is known to bind to cPAH through several side chain contacts, one of which is mediated through three interactions of water with aspartic acid

dx.doi.org/10.1021/bi500734h | Biochemistry 2014, 53, 6834−6848

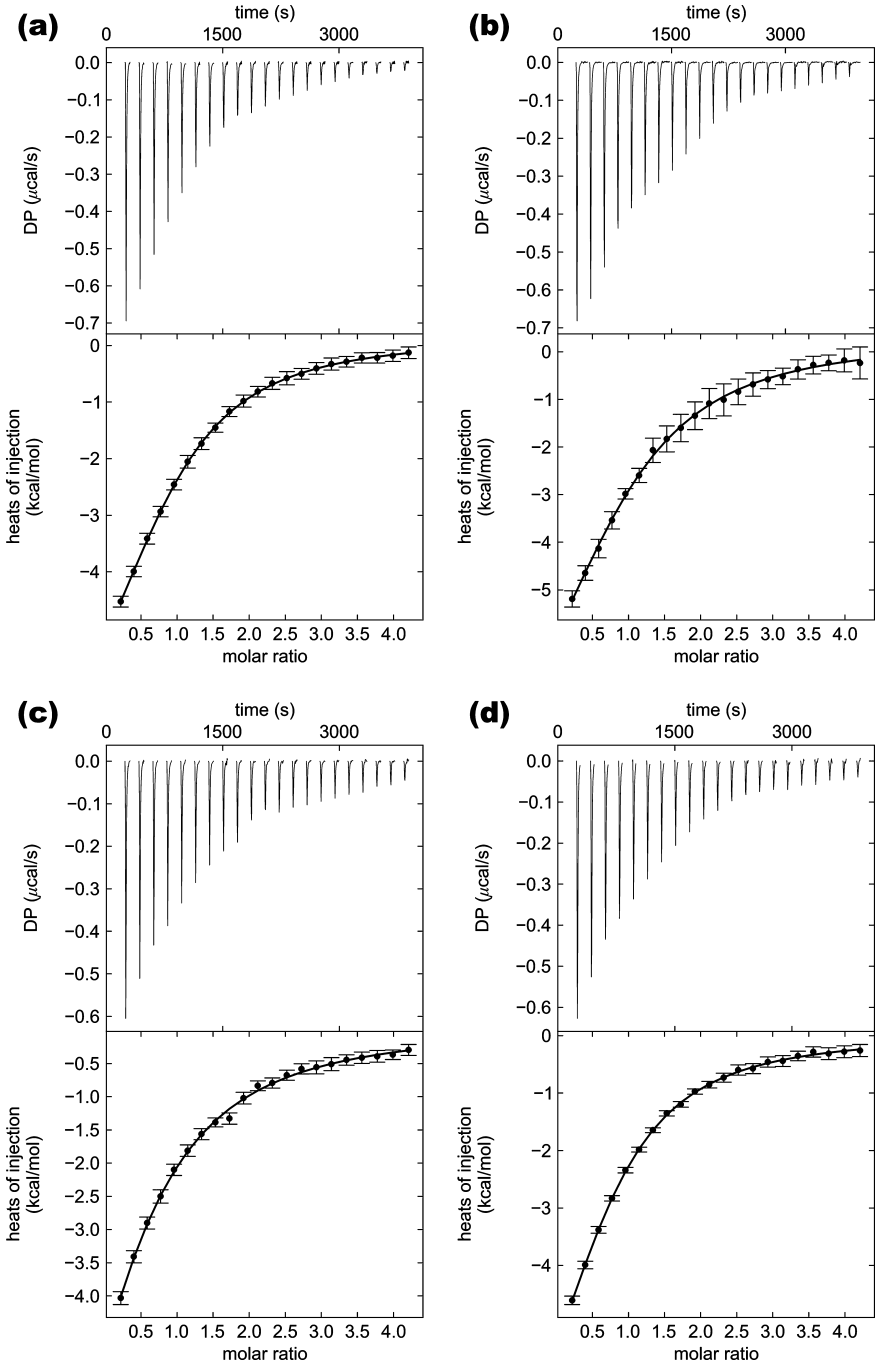

Figure 4. Representative ITC binding isotherms for binding of Phe to (a) D139N, (b) D139A, (c) D139E, and (d) D139K. To keep BH_4 and iron in their reduced form, experiments were conducted under an argon atmosphere.

139. Because the overall crystal structures for the mutants were almost identical to that of the wild-type enzyme, we focused our analysis on the pterin binding pocket of the active site. A hydrogen bond network consisting of waters 1−10 (Figure 5a, PDB entry 3TK4)[31] bridges the active site metal with the carboxylate group of Asp139, the carbonyl group of Pro117, the hydroxyl group of Tyr179, and the carboxylate of E184 (which also coordinates the metal in a bidentate fashion). Because of improved resolution, water molecules constituting this network have been assigned on the basis of the 1.5 Å resolution crystal structure of cPAH bound to Co[31] instead of the 2.0 Å structure of it bound to Fe (PDB entry 1LTV).[15] Binding of pterin in the active site (PDB entry 1LTZ) induces a displacement of waters 6 and 7, due to a steric clash with the O4 atom of the pterin moiety. Waters 9 and 10 are also lost to accommodate the dihydroxypropyl chain of pterin, while a new water molecule is seen hydrogen bonding with both waters 1 and 8 (Figure 5b,c). Since we were unable to obtain structures of the mutants in the pterin-bound state, we focused our analysis on the solvation state of the mutants in their metalated form, prior to binding of the cofactor (Figure 6). The *B* factors for waters contributing to the hydrogen bonding network in the pterin pocket are listed in Table S1 of the Supporting Information. Electron density for active site residues, mutated side chains for D139, and the active site metal are shown in an $F_o - F_c$ simulated annealing omit map contoured at 3σ (Figure 7).

dx.doi.org/10.1021/bi500734h | *Biochemistry* 2014, 53, 6834−6848

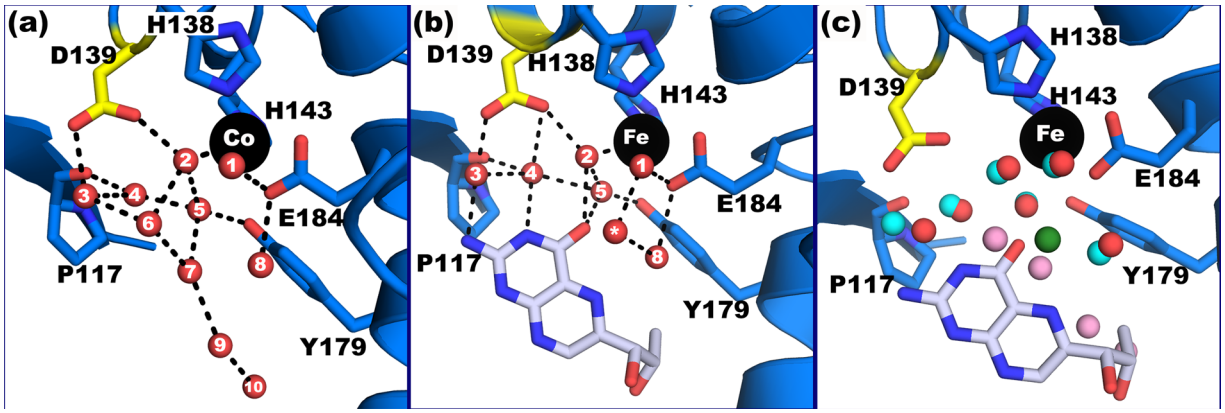

Figure 5. Water network of the pterin binding pocket linking D139 with P117, Y179, and the active site metal of cPAH in the absence (a) and presence (b) of an oxidized form of cofactor 7,8-dihydrobiopterin (BH_2) (PDB entries 3TK4 and 1LTZ). (c) Waters that are lost upon pterin binding are colored pink, while a new water that appears when pterin is bound is colored green. Retained waters from the cofactor-bound structure are colored cyan, while those from the unbound structure are shown as red spheres.

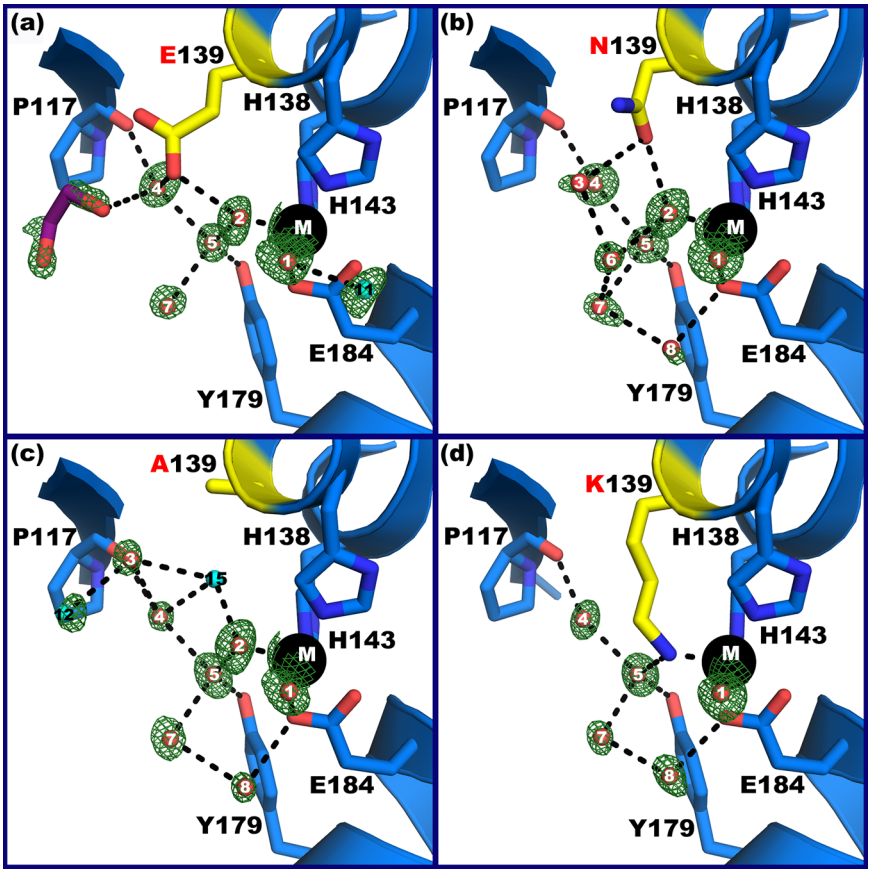

Figure 6. Changes in the water network for Asp139 mutants. Retained waters with respect to the wild type are colored red, while new waters are colored cyan. Density for the waters is colored green and is shown as a simulated annealing omit map contoured at 3σ. The $F_o - F_c$ simulated annealing omit maps were generated by removing all water molecules, the active site metal, and key active site residues from the final model and accordingly refining the model in Phenix[70,71] using simulated annealing parameters in which the protein was heated to 5000 K and subsequently cooled to 300 K in 50 steps at a rate of 100 K/step. (a) The water network for D139E loses water 8 and sees water 3 replaced with ethylene glycol, while (b) the D139N water network is largely unperturbed. (c) In D139A, waters 12 and 15 appear, although the occupancy for water 15 is quite weak. (d) In D139K, the water network is disrupted by loss of water 3, while water 2 is displaced by the ε-amino group of lysine, which coordinates the active site metal. The corresponding $2F_o - F_c$ map after refinement is shown in Figure 6 of the Supporting Information.

The crystal structure of D139E revealed it also retained two of the three waters implicated in pterin binding (Figure 6a). The waters were in the same location as in wild-type cPAH, one that hydrogen bonds with the metal (water 2) and the other forming a 3.0 Å hydrogen bond with the N3 atom of the pteridine ring (water 4). D139E assumes an orientation that positions the carboxylate group away from the metal; the effect of this is registered on the third water, which was displaced by ethylene glycol (used as the cryoprotectant) and moved 2 Å from its normal location to prevent a steric clash with

dx.doi.org/10.1021/bi500734h | *Biochemistry* 2014, 53, 6834−6848

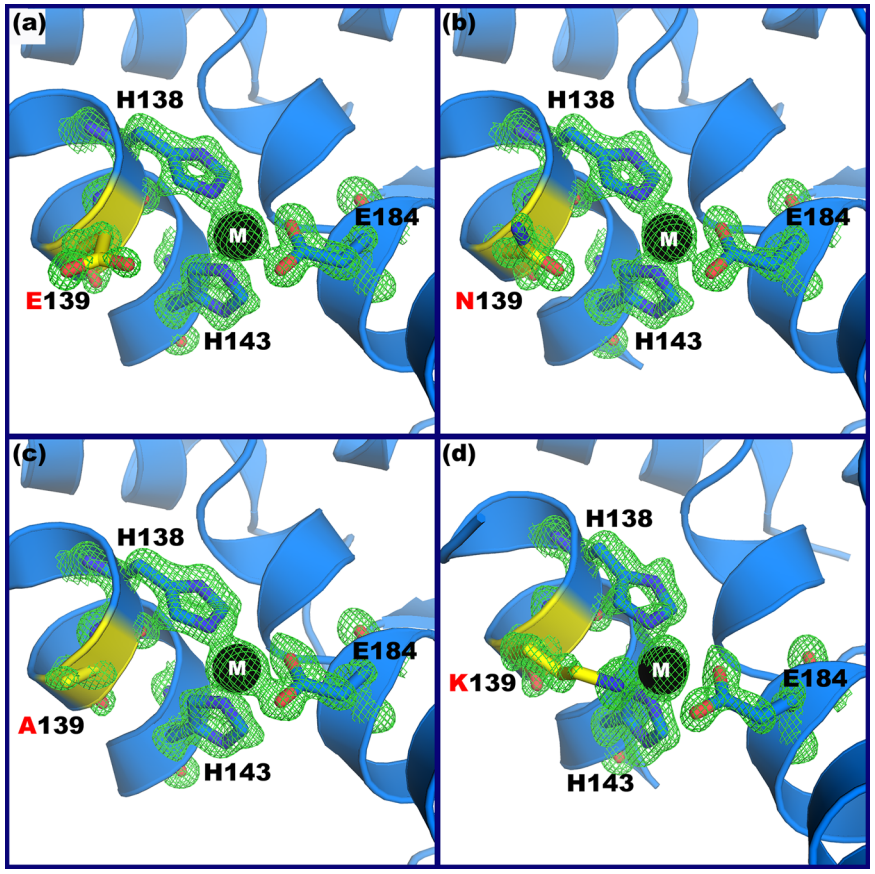

Figure 7. Electron density (colored green) for active site metal-coordinating residues, cobalt (M), and mutant side chains of D139 (colored yellow) for (a) D139E, (b) D139N, (c) D139A, and (d) D139K. The maps shown are $F_o - F_c$ simulated annealing omit maps contoured at 3σ.

glutamate. In aqueous solution, it can be assumed that water would occupy the position taken by ethylene glycol. When water in the D139E structure is modeled in this position with the pterin-bound crystal structure (PDB entry 1LTZ), the distance between that water and the NH_2 group of pterin is just 1.3 Å (Figure 4 of the Supporting Information), indicating that pterin must bind to this enzyme differently or this water would be lost upon its binding. Loss of such an ordered water molecule may contribute, at least in part, to the entropic change we observed upon BH4 binding via ITC.

Interestingly, D139N retains two waters in the exact same location (Figure 6b), one that coordinates with the metal directly (water 2) and another (water 4) that presumably hydrogen bonds with the N3 atom in the pteridine ring at a distance of 2.8 Å. The third water (water 3), which forms a 3.3 Å hydrogen bond with asparagine, while still present, has shifted because the asparagine side chain has adopted an orientation slightly different from that of aspartic acid (the $F_o - F_c$ map contoured at 3.0σ shows weak, but discernible, density for this water, indicating it was somewhat less tightly bound than other clearly visible ones).

Unexpectedly, in D139A, all three waters required for pterin binding were present in the same location as wild-type cPAH, despite a lack of hydrogen bonding partners through side chain contacts at position 139 (Figure 6c). Like the D139E active site, the crystal structure reveals that the active site for the D139A mutant has more water molecules than that of the wild-type enzyme, presumably because of the cavity created upon the mutation. In the D139A mutant, we observed a positive entropic change, ΔS, in ITC experiments upon binding of pterin to D139A, consistent with the crystallographic observation of a more solvated active site.

The crystal structure of D139K reveals that the lysine mutant lacks several waters from the water network. Most noticeably, water 2, which normally coordinates the metal, has been displaced by lysine, which now ligates the metal (Figure 6d; see below). Waters 3 and 6 are also absent from the water network of the lysine mutant. The absence of waters 2 and 3, water molecules that normally bridge Asp and the cofactor, may contribute to the lack of binding seen via ITC, because these waters are needed to stabilize pterin in the active site prior to substrate binding.

Molecular dynamics trajectories allow investigation of the hydrogen bonding and water network in the cPAH active site in the presence of BH_4. We observed strong water-bridged hydrogen bonding between residue 139 and the cofactor in the native system with occupancies of 0.91 and 0.80 for the Fe(II)- and Co(II)-bound systems, respectively. Mutations are consistently found to weaken these interactions. Mutants D139E, D139K, and D139N reduce water-bridged hydrogen bonding to occupancies between 0.05 and 0.37, while D139A in the absence of polar atoms in the side chain shows no hydrogen bonding at all. Direct hydrogen bonding between BH_4 and residue 139 is not observed in the native state. Larger amino acids in mutants D139E and D139K allow some direct interactions in both metal-bound states with occupancies between 0.014 and 0.068.

Changes in hydrogen bonding networks are reflected in alterations in water occupancies (see Figure 5 of the Supporting Information). High occupancies for most water positions in

dx.doi.org/10.1021/bi500734h | *Biochemistry* 2014, 53, 6834−6848

native cPAH are reduced in mutated systems. Coordination to the active site metal prohibits the presence of water 2 in the D139K mutant. We observe partial direct coordination of the side chain carboxylate in D139E with Fe(II); thus, the occupancy of water 2 is reduced similarly. In agreement with data from the D139A crystal structure, we identify a new water positions (water 15) for mutants with small side chains (D139A and D139N). Binding of this additional water molecule is facilitated by hydrogen bonding of the side chain carboxamide to the carbonyl oxygen of D135 [occupancies of 0.69 and 0.78 for Fe(II)- and Co(II)-bound systems, respectively]. This additional hydrogen bond attracts the side chain, thereby creating space for incorporation of an additional water molecule.

Lysine 139 Coordinates the Active Site Metal. Clear electron density of the ε-amino group of lysine in the D139K crystal structure was seen occupying a coordination site on the active site metal (Figure 7d), resulting in displacement of a water molecule that normally ligates the metal. Octahedral coordination of the metal is still achieved, despite a loss of this water molecule, because the other ligands remain in place. Remarkably, mutation of Asp139 to lysine resulted in it assuming the role of a first-coordination sphere ligand of the active site metal, instead of its usual role in the enzyme's second-coordination sphere (as a residue that is indirectly attached to a metal's ligand, in this case, water). Of added interest is the fact that, despite a complete lack of activity and, most importantly, significantly impaired iron binding as judged by ITC, strong density in the $2F_o - F_c$ map corresponding to bound metal is visible in the active site. One possible explanation for this is that the lysine mutant has greater affinity for an inhibitory metal such as cobalt (used in the crystallization buffer) rather than iron.[57] Alternatively, the metal-bound species of the Lys mutant could be a minor population in solution, but one that has crystallized preferentially over the major, nonmetalated species. The kinetic and binding results with the lysine mutant may reflect a steric clash with the cofactor, despite our observation in crystals that it could be oriented toward the metal center. In solution, in the presence of the native metal, the side chain of lysine may not be engaged completely or at all with the metal, as indicated by ITC data, and can prevent cofactor binding either by direct steric clash or by preventing the formation of the water bridge.

This observation was striking since lysine is widely regarded as a poor ligand for metals. Typically, coordination of lysine with active site metals occurs in one of two ways: either through its backbone carbonyl oxygen atom or through a carbamylated lysine (a post-translational modification in which lysine's ε-amino group is carboxylated).[58,59] In fact, direct coordination of the ε-amino group with a transition metal is rare. One such example is the 1.6 Å crystal structure of the zinc metalloprotein leucine amino peptidase (PDB entry 1LAM),[60] which reveals a binuclear zinc active site in which one of the zinc atoms is ligated by a nearby lysine (Figure 7 of the Supporting Information). Both the 3.0 and 1.95 Å crystal structures of ubiquitin (PDB entry 3H1U)[61] and lysine 63-linked diubiquitin (PDB entry 2JF5)[62] reveal that one of the surface lysine residues of ubiquitin (Lys29) can coordinate cadmium (Figure 7 of the Supporting Information). Similar to the D139K mutant of cPAH described in the present study, artifactual lysine metal coordination has also been observed in other systems, such as by replacement of the copper-coordinating methionine in amicyanin with lysine, yielding an enzyme that binds zinc instead of copper (PDB entry 3RYM),[63] and by mutation of the axial heme iron methionine ligand in a bacterial cytochrome c_{550} enzyme, leading to coordination of the amino group of lysine with the heme iron (PDB entry 2BH5).[64]

DISCUSSION

The high-resolution crystal structure of cPAH in complex with the oxidized form of its cofactor, BH_2,[15] in addition to crystal structures of other AAAHs,[16−19,25,26] shows an acidic amino acid in the enzyme's second coordination sphere engaged in numerous hydrogen bonding interactions. Specifically, in cPAH the carboxylate of D139 lies 4.2 Å from the iron; however, it utilizes a water molecule near the iron to form hydrogen bonds both with iron and with the O4 atom of BH_2. Likewise, the equivalent residues in human PAH (E286), rat TH (E332), and human TPH (E273) all reside 4.4 Å from the active site iron. Because this residue is located close to the metal, it is reasonable to propose that the charge it carries has a role in catalysis, perhaps through stabilization of iron. We used ITC as a measure of direct metal binding in the active site of wild-type cPAH and the D139 mutants studied here. Replacing a carboxylate side chain with a carboxamide group (D139N) does not appear to have an effect with respect to metal binding (if anything, the protein's affinity for iron was slightly improved). However, removal of the polar atoms from the side chain completely through the introduction of alanine at position 139 in cPAH impairs the enzyme's ability to bind iron. While the presence of a polar side chain at position 139 seems to be important for metal binding, the size of the side chain is also important. Introduction of an additional CH_2 and thus increasing the side chain's conformational entropy by mutating Asp to Glu lead to a decreased affinity for iron even though the charge is the same. This is consistent with the side chain playing a role in binding the metal, but the charge is not the only important factor in this binding.

The aforementioned crystal structure of cPAH in complex with BH_2 shows three hydrogen bonds, bridged by three water molecules, between D139 and the NH_2, N3, and O4 atoms in the pteridine ring of BH_2, suggesting that D139 contributes to catalysis by properly orienting the cofactor. Previous kinetic studies of the D139 equivalent residue in two different N-terminal regulatory domain-deleted constructs of hPAH led to the conclusion that this residue plays a key role in positioning of the cofactor for catalysis.[17,32] One of the studies[32] found that mutation of E286 to alanine led to an increase in K_M for pterin, while mutation to glutamine did not change the K_M of pterin. Our kinetic results (Table 2) do not reflect a change in the K_M of pterin in D139A or D139N; however, a drastic change in k_{cat} was observed in each mutant. To understand how changes in polarity and charge to D139 affected pterin binding, we used ITC to directly measure each mutant's affinity for pterin. These studies indicate that the negative charge conveyed by the Asp residue contributes to stronger binding with the cofactor, possibly through strong hydrogen bonding with the bridging waters. The trend observed in pterin binding in the wild-type enzyme and the D139N and D139A mutants mirrored the trend in k_{cat} values; however, the magnitude of the change in k_{cat} is significantly more substantial than the effect on pterin affinity. A possible explanation for the enhanced binding ability in the D139E mutant for BH_4 is that the cofactor has bound somewhat directly to the side chain, instead of indirectly through water-mediated contacts. Molecular dynamics data

dx.doi.org/10.1021/bi500734h | Biochemistry 2014, 53, 6834−6848

support this view by showing stronger intermolecular interactions and some extent of direct hydrogen bonding. If this is so, it may explain why the D139E enzyme is less active than the wild-type enzyme; the elimination of some water-mediated contacts in favor of direct contacts between the cofactor and the glutamate side chain leading to tighter binding between the two could mean that the cofactor is trapped in an arrangement making it more difficult to undergo the transition to the productive orientation required for catalysis in the presence of Phe. Alternatively, it could also mean that the cofactor is likely assuming an orientation similar to the productive form of pterin binding in the absence of phenylalanine. This repositioning of the cofactor in the active site is counterproductive for the enzyme because typically hydroxylation of phenylalanine to tyrosine is tightly coupled with oxidation of the cofactor; however, a second, uncoupled, pathway is known to occur without forming product, in which BH_4 can be directly oxidized to quinonoid dihydropterin, generating H_2O_2.[65] This effect was observed in a previous study of PAH mutants that induce PKU[66] and other studies using analogues of the substrate or cofactor.[2,67]

Altogether, our results seem to indicate that the conserved acidic side chain plays a more prominent role in stabilizing the transition state by placing pterin in a productive orientation with respect to the metal center, most likely by direct hydrogen bonding. Such hydrogen bonding involving the negative charge on the side chain could make a more substantial contribution to pterin binding than indirect interactions involving the bridging waters. These results are also consistent with a model of pterin hydroxylation that proposes that the carboxylate group of E286 (D139 in cPAH) may function to "stabilize the positive charge delocalized in the pyrimidine ring of the peroxy−pterin intermediate."[33]

Our results highlight the importance of the bridging water molecules in catalysis. The placement of these water molecules between the side chain of Asp139 and the cofactor prevents direct contact between the two, presumably preventing uncoupled hydroxylation of the cofactor. It is interesting to note that these bridging water molecules, although supported by Asp139, are more dependent on the metal for their existence (the crystal structures of the Asn and Ala mutants show many of these are retained). This dependence on the metal, particularly on one of the waters that is directly coordinated to it, confers a distinct advantage: when oxygen binds, it would displace the key water from the coordination sphere of the metal, which would deform the network of hydrogen bonds, leading to facile expulsion of the bridging waters en route to the transition state. After completion of the reaction cycle, the water structure around the metal and the acidic side chain would be reestablished. These intervening waters would weaken the oxidized cofactor, leading to its departure from the active site. Thus, the bridging waters may also facilitate release of the oxidized cofactor.

Molecular dynamics data strengthen these hypotheses, as we observe a strong hydrogen bonding network in the native system, including solvent-bridged hydrogen bonds between residue 139 and the cofactor. Mutations to larger residues (D139E and D139K) partially break the formed water structures, partially compensated by direct hydrogen bonding between the cofactor and the amino acid side chain. These additional interactions might impair release of the oxidized cofactor.

In conclusion, we have shown that the mutations of aspartic acid 139 in the second coordination sphere of cPAH do not affect the enzyme's ability to bind its substrate, phenylalanine, but instead influence both iron and cofactor binding. Previously, it was suggested that an inhibitory complex forms between hPAH and BH_4 requiring its own dissociation prior to phenylalanine activation.[68] Along those lines, recently a kinetic study by Roberts et al.[69] proposed that PAH can form two different pterin complexes: one that orients BH_4 in an unproductive form and another that orients it in a catalytically productive form. Our studies are in agreement with this idea. The acidic amino acid is essential to proper enzymatic function, because it not only is important in stabilizing the cofactor properly through bridging water molecules in the ground state (unproductive form) but also plays an important role in stabilizing the putative peroxy−pterin intermediate in the transition state.

■ ASSOCIATED CONTENT

Ⓢ Supporting Information

Supporting Figures 1−7 and Table S1. This material is available free of charge via the Internet at http://pubs.acs.org.

Accession Codes

Coordinates and structure factors have been deposited in the PDB as entries 4Q3W (D139E), 4Q3X (D139N), 4Q3Y (D139A), and 4Q3Z (D139K).

■ AUTHOR INFORMATION

Corresponding Author

*Brown Laboratory of Chemistry, Purdue University, 560 Oval Dr., West Lafayette, IN 47907. E-mail: cdas@purdue.edu. Phone: (765) 494-5478. Fax: (765) 494-0239.

Funding

This research was funded by the National Science Foundation (Grant CHE-0749572 to M.M.A.-O.) and the National Institutes of Health (Grant 1R01RR026273 to C.D.).

Notes

The authors declare no competing financial interest.

■ ACKNOWLEDGMENTS

We are grateful to our hosts Craig Ogata, Nagarajan Venugopalan, and Ruslan Sanishvili at GM/CA CAT beamlines 23-ID-D and 23-ID-B at the Advanced Photon Source at Argonne National Laboratory. Use of the Advanced Photon Source, an Office of Science User Facility operated for the U.S. Department of Energy (DOE) Office of Science by Argonne National Laboratory, was supported by the U.S. DOE under Contract DE-AC02-06CH11357.

■ REFERENCES

(1) Hufton, S. E., Jennings, G., and Cotton, R. G. H. (1995) Structure and function of the aromatic amino acid hydroxylases. *Biochem. J. 311*, 353−366.

(2) Kappock, T. J., and Caradonna, J. P. (1996) Pterin-dependent amino acid hydroxylases. *Chem. Rev. 96*, 2659−2756.

(3) Kaufman, S. (1993) The phenylalanine hydroxylating system. *Adv. Enzymol. Relat. Areas Mol. Biol. 67*, 77−264.

(4) Abu-Omar, M. M., Loaiza, A., and Hontzeas, N. (2005) Reaction mechanisms of mononuclear non-heme iron oxygenases. *Chem. Rev. 105*, 2227−2252.

(5) Flatmark, T., and Stevens, R. C. (1999) Structural Insight into the Aromatic Amino Acid Hydroxylases and Their Disease-Related Mutant Forms. *Chem. Rev. 99*, 2137−2160.

(6) Hegg, E. L., and Que, L. (1997) The 2-His-1-carboxylate facial triad: An emerging structural motif in mononuclear non-heme iron(II) enzymes. *Eur. J. Biochem. 250*, 625−629.
(7) Fitzpatrick, P. F. (1999) Tetrahydropterin-Dependent Amino Acid Hydroxylases. *Annu. Rev. Biochem. 68*, 355−381.
(8) Rebrin, I., Bailey, S. W., Boerth, S. R., Ardell, M. D., and Ayling, J. E. (1995) Catalytic characterization of a 4a-Hydroxytetrahydropterin Dehydratase. *Biochemistry 34*, 5801−5810.
(9) Kumer, S. C., and Vrana, K. E. (2002) Intricate Regulation of Tyrosine Hydroxylase Activity and Gene Expression. *J. Neurochem. 67*, 443−462.
(10) Flydal, M. I., and Martinez, A. (2013) Phenylalanine hydroxylase: Function, structure, and regulation. *IUBMB Life 65*, 341−349.
(11) Matthews, D. E. (2007) An overview of phenylalanine and tyrosine kinetics in humans. *J. Nutr. 137*, 15494−15555.
(12) Kaufman, S. (1999) A model of human phenylalanine metabolism in normal subjects and in phenylketonuric patients. *Proc. Natl. Acad. Sci. U.S.A. 96*, 3160−3164.
(13) Scriver, C. R. (1995) Whatever happened to PKU? *Clin. Biochem. 28*, 137−144.
(14) Williams, R. A., Mamotte, C. D. S., and Burnett, J. R. (2008) Phenylketonuria: An Inborn Error of Phenylalanine Metabolism. *Clin. Biochem. Rev. 29*, 31−41.
(15) Erlandsen, H., Kim, J. Y., Patch, M. G., Han, A., Volner, A., Abu-Omar, M. M., and Stevens, R. C. (2002) Structural Comparison of Bacterial and Human Iron-dependent Phenylalanine Hydroxylase: Similar Fold, Different Stability and Reaction Rates. *J. Mol. Biol. 320*, 645−661.
(16) Andersen, O. A., Stokka, A. J., Flatmark, T., and Hough, E. (2003) 2.0 Å Resolution Crystal Structures of the Ternary Complexes of Human Phenylalanine Hydroxylase Catalytic Domain with Tetrahydrobiopterin and 3-(2-Thienyl)-L-alanine or L-Norleucine: Substrate Specificity and Molecular Motions Related to Substrate Binding. *J. Mol. Biol. 333*, 747−757.
(17) Erlandsen, H., Bjørgo, E., Flatmark, T., and Stevens, R. C. (2000) Crystal Structure and Site-Specific Mutagenesis of Pterin-Bound Human Phenylalanine Hydroxylase. *Biochemistry 39*, 2208−2217.
(18) Goodwill, K. E., Sabatier, C., Marks, C., Raag, R., Fitzpatrick, P. F., and Stevens, R. C. (1997) Crystal structure of tyrosine hydroxylase at 2.3 Å and its implications for inherited neurodegenerative diseases. *Nat. Struct. Biol. 4*, 578−585.
(19) Goodwill, K. E., Sabatier, C., and Stevens, R. C. (1998) Crystal structure of tyrosine hydroxylase with bound cofactor analogue and iron at 2.3 Å resolution: Self-hydroxylation of Phe300 and the pterin-binding site. *Biochemistry 37*, 13437−13445.
(20) Wang, L., Erlandsen, H., Haavik, J., Knappskog, P. M., and Stevens, R. C. (2002) Three-dimensional structure of human tryptophan hydroxylase and its implications for the biosynthesis of the neurotransmitters serotonin and melatonin. *Biochemistry 41*, 12569−12574.
(21) Jennings, I. G., Kemp, B. E., and Cotton, R. G. H. (1991) Localization of cofactor binding sites with monoclonal anti-idiotype antibodies: Phenylalanine hydroxylase. *Proc. Natl. Acad. Sci. U.S.A. 88*, 5734−5738.
(22) Zoidakis, J., Sam, M., Volner, A., Han, A., Vu, K., and Abu-Omar, M. M. (2004) Role of the second coordination sphere residue tyrosine 179 in substrate affinity and catalytic activity of phenylalanine hydroxylase. *JBIC, J. Biol. Inorg. Chem. 9*, 289−296.
(23) Kinzie, S. D., Thevis, M., Ngo, K., Whitelegge, J., Loo, J. A., and Abu-Omar, M. M. (2003) Posttranslational Hydroxylation of Human Phenylalanine Hydroxylase Is a Novel Example of Enzyme Self-Rpair within the Second Coordination Sphere of Catalytic Iron. *J. Am. Chem. Soc. 125*, 4710−4711.
(24) Miranda, F. F., Kolber, M., Andersson, K. K., Geraldes, C. F., and Martinez, A. (2005) The active site residue tyrosine 325 influences iron binding and coupling efficiency in human phenylalanine hydroxylase. *J. Inorg. Biochem. 99*, 1320−1328.
(25) Andersen, O. A., Flatmark, T., and Hough, E. (2001) High resolution crystal structures of the catalytic domain of human phenylalanine hydroxylase in its catalytically active Fe(II) form and binary complex with tetrahydrobiopterin. *J. Mol. Biol. 314*, 279−291.
(26) Andersen, O. A., Flatmark, T., and Hough, E. (2002) Crystal structure of the ternary complex of the catalytic domain of human phenylalanine hydroxylase with tetrahydrobiopterin and 3-(2-thienyl)-L-alanine, and its implications for the mechanism of catalysis and substrate activation. *J. Mol. Biol. 320*, 1095−1108.
(27) Fusetti, F., Erlandsen, H., Flatmark, T., and Stevens, R. C. (1998) Structure of the tetrameric human phenylalanine hydroxylase and its implications for phenylketonuria. *J. Biol. Chem. 273*, 16962−16967.
(28) Loaiza, A., Armstrong, K. M., Baker, B. M., and Abu-Omar, M. M. (2008) Kinetics of thermal unfolding of phenylalanine hydroxylase variants containing different metal cofactors (Fe^{II}, Co^{II}, and Zn^{II}) and their isokinetic relationship. *Inorg. Chem. 47*, 4877−4883.
(29) Fitzpatrick, P. F. (2012) Allosteric regulation of phenylalanine hydroxylase. *Arch. Biochem. Biophys. 519*, 194−201.
(30) Volner, A., Zoidakis, J., and Abu-Omar, M. M. (2003) Order of substrate binding in bacterial phenylalanine hydroxylase and its mechanistic implication for pterin-dependent oxygenases. *JBIC, J. Biol. Inorg. Chem. 8*, 121−128.
(31) Ronau, J. A., Paul, L. N., Fuchs, J. E., Corn, I. R., Wagner, K. T., Liedl, K. R., Abu-Omar, M. M., and Das, C. (2013) An additional substrate binding site in a bacterial phenylalanine hydroxylase. *Eur. Biophys. J. 42*, 691−708.
(32) Dickson, P. W., Jennings, I. G., and Cotton, R. G. H. (1994) Delineation of the Catalytic Core of Phenylalanine Hydroxylase and Identification of Glutamate 286 as a Critical Residue for Pterin Function. *J. Biol. Chem. 269*, 20369−20375.
(33) Bassan, A., Borowski, T., and Siegbahn, P. E. M. (2004) Quantum chemical studies of dioxygen activation by mononuclear non-heme iron enzymes with the 2-His-1-carboxylate facial triad. *Dalton Trans.*, 3153−3162.
(34) Otwinowski, Z., and Minor, W. (1997) Processing of X-ray Diffraction Data Collected in Oscillation Mode. In *Methods in Enzymology, Macromolecular Crystallography, Part A* (Carter, C. W., Jr., and Sweet, R. M., Eds.) Academic Press, New York.
(35) Vagin, A., and Teplyakov, A. (1997) MOLREP: An Automated Program for Molecular Replacement. *J. Appl. Crystallogr. 30*, 1022−1025.
(36) Collaborative Computational Project, Number 4 (1994) The CCP4 suite: Programs for protein crystallography. *Acta Crystallogr. D50*, 760−763.
(37) Murshudov, G. N., Skubak, P., Lebedev, A. A., Pannu, N. S., Steiner, R. A., Nicholls, R. A., Winn, M. D., Long, F., and Vagin, A. A. (2011) REFMAC5 for the refinement of macromolecular crystal structures. *Acta Crystallogr. D67*, 355−367.
(38) Emsley, P., Lohkamp, B., Scott, W. G., and Cowtan, K. (2010) Features and development of Coot. *Acta Crystallogr. D66*, 486−501.
(39) *The PyMOL Molecular Graphics System*, Version 1.5.0.4 Schrödinger, LLC.
(40) Labute, P. (2009) Protonate3D: Assignment of ionization states and hydrogen coordinates to macromolecular structures. *Proteins 75*, 187−205.
(41) Jorgensen, W. L., Chandrasekhar, J., Madura, J. D., Impey, R. W., and Klein, M. L. (1983) Comparison of simple potential functions for simulating liquid water. *J. Chem. Phys. 79*, 926−935.
(42) Salomon-Ferrer, R., Goetz, A. W., Poole, D., Le Grand, S., and Walker, R. C. (2013) Routine microsecond molecular dynamics simulation with AMBER-Part II: Particle Mesh Ewald. *J. Chem. Theory Comput. 9*, 3878−3888.
(43) Case, D. A., et al. (2014) *AMBER 14*, University of California, San Francisco.
(44) Lindorff-Larsen, K., Piana, S., Palmo, K., Maragakis, P., Klepeis, J. L., Dror, R. O., and Shaw, D. E. (2010) Improved side-chain torsion potentials for the Amber ff99SB protein force field. *Proteins 78*, 1950−1958.

(45) Wang, J., Wolf, R. M., Caldwell, J. W., Kollman, P. A., and Case, D. A. (2004) Development and testing of a general amber force field. *J. Comput. Chem. 25*, 1157−1174.
(46) Fuchs, J. E., Fuchs, D., and Liedl, K. R. (2014) Dynamic regulation of phenylalanine hydroxylase. *Pteridines 2*, 33−39.
(47) Fuchs, J. E., Huber, R. G., von Grafenstein, S., Wallnoefer, H. G., Spitzer, G. M., Fuchs, D., and Liedl, K. R. (2012) Dynamic regulation of phenylalanine hydroxylase by simulated redox manipulation. *PLoS One 7*, e53005.
(48) Frisch, M. J., et al. (2004) *Gaussian03*, revision C.02, Gaussian Inc., Wallingford, CT.
(49) Ciccotti, G., and Ryckaert, J. P. (1986) Molecular Dynamics Simulations of Rigid Molecules. *Comput. Phys. Rep. 64*, 2375−2388.
(50) Wallnoefer, H. G., Handschuh, S., Liedl, K. R., and Fox, T. (2010) Stabilizing of a globular protein by a highly complex water network: A molecular dynamics simulation study on factor Xa. *J. Phys. Chem. B 114*, 7405−7412.
(51) Roe, D. R., and Cheatham, T. E., III (2013) PTRAJ and CPPTRAJ: Software for Processing and Analysis of Molecular Dynamics Trajectory Data. *J. Chem. Theory Comput. 9*, 3084−3095.
(52) Keller, S., Vargas, C., Zhao, H., Piszczek, G., Brautigam, C. A., and Schuck, P. (2012) High-precision isothermal titration calorimetry with automated peak-shape analysis. *Anal. Chem. 84*, 5066−5073.
(53) Houtman, J. C., Brown, P. H., Bowden, B., Yamaguchi, H., Appella, E., Samelson, L. E., and Schuck, P. (2007) Studying multisite binary and ternary protein interactions by global analysis of isothermal titration calorimetry data in SEDPHAT: Application to adaptor protein complexes in cell signaling. *Protein Sci. 16*, 30−42.
(54) Vistica, J., Dam, J., Balbo, A., Yikilmaz, E., Mariuzza, R. A., Rouault, T. A., and Schuck, P. (2004) Sedimentation equilibrium analysis of protein interactions with global implicit mass conservation constraints and systematic noise decomposition. *Anal. Biochem. 326*, 234−256.
(55) Bronowska, A. K. (2011) Thermodynamics of Ligand-Protein Interactions: Implications for Molecular Design. In *Thermodynamics-Interaction Studies-Solids, Liquids and Gases* (Moreno PirajÃin, J. C., Ed.) InTech, Rijeka, Croatia.
(56) Jelesarov, I., and Bosshard, H. R. (1999) Isothermal titration calorimetry and differential scanning calorimetry as complementary tools to investigate the energetics of biomolecular recognition. *J. Mol. Recognit. 12*, 3−18.
(57) Zoidakis, J., Loaiza, A., Vu, K., and Abu-Omar, M. M. (2005) Effect of temperature, pH, and metals on the stability and activity of phenylalanine hydroxylase from *Chromobacterium violaceum*. *J. Inorg. Biochem. 99*, 771−775.
(58) Holm, R. H., Kennepohi, P., and Solomon, E. I. (1996) Structural and Functional Aspects of Metal Sites in Biology. *Chem. Rev. 96*, 2239−2314.
(59) Laitaoja, M., Valijakka, J., and Jänis, J. (2013) Zinc coordination spheres in protein structures. *Inorg. Chem. 52*, 10983−10991.
(60) Sträter, N., and Lipscomb, W. N. (1995) Two-metal ion mechanism of bovine lens leucine aminopeptidase: Active site solvent structure and binding mode of L-leucinal, a gem-diolate transition state analogue, by X-ray crystallography. *Biochemistry 34*, 14792−14800.
(61) Qureshi, I. A., Ferron, F., Seh, C. C., Cheung, P., and Lescar, J. (2009) Crystallographic structure of ubiquitin in complex with cadmium ions. *BMC Res. Notes 2*, 251.
(62) Komander, D., Reyes-Turcu, F., Licchesi, J. D., Odenwaelder, P., Wilkinson, K. D., and Barford, D. (2009) Molecular discrimination of structurally equivalent Lys 63-linked and linear polyubiquitin chains. *EMBO Rep. 10*, 466−473.
(63) Sukumar, N., Choi, M., and Davidson, V. L. (2011) Replacement of the axial copper ligand methionine with lysine in amicyanin converts it to a zinc-binding protein that no longer binds copper. *J. Inorg. Biochem. 105*, 1638−1644.
(64) Worrall, J. A., van Roon, A. M., Ubbink, M., and Canters, G. W. (2005) The effect of replacing the axial methionine ligand with a lysine residue in cytochrome c-550 from *Paracoccus versutus* assessed by X-ray crystallography and unfolding. *FEBS J. 272*, 2441−2455.
(65) Dix, T. A., and Benkovic, S. J. (1985) Mechanism of "uncoupled" tetrahydropterin oxidation by phenylalanine hydroxylase. *Biochemistry 24*, 5839−5846.
(66) Kemsley, J. N., Wasinger, E. C., Datta, S., Mitić, N., Acharya, T., Hedman, B., Caradonna, J. P., Hodgson, K. O., and Solomon, E. I. (2003) Spectroscopic and kinetic studies of PKU-inducing mutants of phenylalanine hydroxylase: Arg158Gln and Glu280Lys. *J. Am. Chem. Soc. 125*, 5677−5686.
(67) Marota, J. J., and Shiman, R. (1984) Stoichiometric reduction of phenylalanine hydroxylase by its cofactor: A requirement for enzymatic activity. *Biochemistry 23*, 1303−1311.
(68) Xia, T., Gray, D. W., and Shiman, R. (1994) Regulation of rat liver phenylalanine hydroxylase. III. Control of catalysis by (6R)-tetrahydrobiopterin and phenylalanine. *J. Biol. Chem. 269*, 24657−24665.
(69) Roberts, K. M., Pavon, J. A., and Fitzpatrick, P. F. (2013) Kinetic Mechanism of Phenylalanine Hydroxylase: Intrinsic Binding and Rate Constants from Single-Turnover Experiments. *Biochemistry 52*, 1062−1073.
(70) Adams, P. D., Afonine, P. V., Bunkoczi, G., Chen, V. B., Davis, I. W., Echols, N., Headd, J. J., Hung, L.-W., Kapral, G. J., and Grosse-Kunstleve, R. W. (2010) PHENIX: A comprehensive Python-based system for macromolecular structure solution. *Acta Crystallogr. D66*, 213−221.
(71) Adams, P. D., Grosse-Kunstleve, R. W., Hung, L. W., Ioerger, T. R., McCoy, A. J., Moriarty, N. W., Read, R. J., Sacchettini, J. C., Sauter, N. K., and Terwilliger, T. C. (2002) PHENIX: Building new software for automated crystallographic structure determination. *Acta Crystallogr. D58*, 1948−1954.